

Microwave Assisted Synthesis of Stable and Highly Active Ir-oxohydroxides for Electrochemical Oxidation of Water

Cyriac Massué^[a,b], Xing Huang^[a], Andrey Tarasov^[a], Chinmoy Ranjan^[b], Sébastien Cap^{*[a]} and Robert Schlögl^[a,b]

Abstract: Water splitting for hydrogen production in acidic media has been limited by the poor stability of the anodic electrocatalyst devoted to the oxygen evolution reaction (OER). To help circumvent this problem we have synthesized a class of novel Ir-oxohydroxides via rapid microwave-supported hydrothermal synthesis, which bridge the gap between electrodeposited amorphous IrO_x-films and crystalline IrO₂-electrocatalysts prepared via calcination routes. For electrode loadings two orders of magnitude below current standards, the synthesized compounds present an unrivalled combination of high activity and stability under commercially relevant OER-conditions in comparison to reported benchmarks, without any need for pre-treatment. The best compound achieved a lifetime 33 times longer than the best commercial Ir-benchmark. Thus, the reported efficient synthesis of an Ir-oxohydroxide phase with superior intrinsic OER-performance constitutes a major step towards the targeted design of cost-efficient Ir-based OER-electrocatalysts for acidic media.

Introduction

Hydrogen formation via water splitting remains the only long term solution for stable and versatile storage of renewable electricity in chemical form.^[1] Proton exchange membrane (PEM) based electrolyzers offer efficient operating conditions with the possibility to produce high-purity H₂ at elevated pressures.^[2] Such electrolyzers are based on polymeric membranes with proton exchange capabilities, e.g., Nafion, which act as a gas separator between the anodic and cathodic compartments. These proton-conducting membranes rely on sulfonic-acid chemical groups, which require highly acidic pH-conditions. Such a working regime imposes a harsh chemical environment onto the water splitting catalysts. Particularly the anode, where the oxygen evolution reaction (OER) takes place has to withstand a severely corrosive environment.^[3] Most earth-abundant transition metal oxides such as Co₃O₄, Fe₂O₃ and MnO_x show minimal OER-stability in acidic electrolytes.^[2] So far, only Ir-based catalysts are reported to combine high activity with relative stability in acidic OER.^[4]

Ir is an outstanding candidate for acidic OER-electrocatalysis. However due to the scarcity of Ir^[5] it is desirable to minimize electrode loadings by optimizing the intrinsic electrochemical

OER-performance of Ir-based catalysts. In this regard, achieving the right chemical state of Ir has been pointed out to be of prime importance. Early on, Beni et al. showed that metallic iridium films constitute inefficient OER-catalysts and need to be activated by an oxidative electrochemical treatment.^[6] Accordingly, synthesis strategies were developed for the direct formation of OER-active Ir-films such as anodically grown iridium oxide films^[7,8] (AIROF) or sputtered iridium oxide films^[6] (SIROF). In these studies the authors emphasized the key role of amorphous Ir-oxohydroxides in high-current, stable OER-electrocatalysis in contrast to the less active crystalline IrO₂.^[6–8] However, most recent studies have focused on the calcination-based synthesis of crystalline IrO₂ and mixed Ir-oxides, e.g. IrO₂/Ta₂O₅.^[3,9–12] This focus is related to the popular notion that crystalline IrO₂-rutile is the most promising candidate in terms of long-term OER-stability.^[3,13] Nonetheless, the relevance of highly hydroxylated Ir-species was further established by the electrochemical investigation of Ir-catalysts produced at low calcination temperatures by P. Strasser's and K. Mayrhofer's teams.^[14,15] Their work showed that Ir-acetates calcined at the lowest possible decomposition temperature of 250 °C formed amorphous Ir-oxide/hydroxide-species, combining both activity and stability in acidic OER, whereas the OER-performance of crystalline IrO₂ produced at higher temperature was clearly inferior. Most recently, Pfeifer et al. investigated the electronic structure of active Ir-oxide based catalysts and confirmed the superior OER-performance of amorphous Ir^{III/IV}-oxohydroxides in comparison with IrO₂.^[16,17] The superior intrinsic activity of Ir^{III/IV}-oxohydroxides was linked to their ability to accommodate nucleophilic reactive oxygen species.^[18]

The numerous clues about the OER-relevance of amorphous or nanocrystalline Ir-oxohydroxide-type species are a strong incentive to develop a rational approach to the synthesis of such compounds. For this purpose, we designed a synthesis strategy using a microwave (MW)-assisted hydrothermal setup, allowing for the thermal treatment of aqueous precursor solutions at temperatures of 250 °C or below. Such an approach circumvents the classical synthesis strategies mostly relying on calcination steps under dry conditions above 250°C, which often lead to the formation of crystalline IrO₂. By using the MW-assisted hydrothermal treatment, a series of Ir-based electrocatalysts was obtained by varying the relative ratio of the two main reactants, potassium hydroxide (KOH) and Ir-precursor (K₂IrCl₆). The chemical composition of the Ir-compounds in terms of oxidation, hydroxylation and atomic ratios was characterized using well established methods. OER performance metrics, i.e., activity and stability, of each compound were quantified and compared to literature references as well as to two commercially available Ir-benchmarks: crystalline IrO₂ (Sigma-Aldrich), denoted SA-IrO₂ and a quasi-amorphous ultra-pure Ir-oxohydroxide (Alfa Aesar) denoted AA-IrO_x used in previous studies as the most performant commercial pure Ir-based OER-catalyst available.^[16–18]

The aim of the present study is to highlight a novel systematic synthesis approach to the promising class of Ir-oxohydroxides for OER-electrocatalysis. Functional relationships were investigated by relating variations in sample composition and chemical nature to changes in OER-performance. Thus, the

[a] Prof. Dr. R. Schlögl, Dr. C. Massué, Dr. S. Cap, Dr. X. Huang, Dr. A. Tarasov
Department of Inorganic Chemistry
Fritz-Haber-Institute of the Max-Planck Society
Berlin 14195, Germany
E-mail: sebastien.cap@fhi-berlin.mpg.de

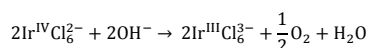
[b] Prof. Dr. R. Schlögl, Dr. C. Massué, Dr. C. Ranjan
Department of Heterogenous Reactions
Max-Planck Institute for Chemical Energy Conversion
Mülheim-an-der-Ruhr 45470, Germany

Supporting information for this article is given via a link at the end of the document.

identification of OER-relevant features controlled by the synthetic parameters of our MW-assisted hydrothermal synthesis will allow for a targeted approach to the preparation of Ir-based catalysts featuring superior OER-performance.

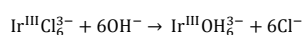
Results and Discussion

Catalyst synthesis. — In the present study a MW-supported hydrothermal synthesis strategy was chosen as MW-supported heating allows for fast heating ramps, shorter synthesis times than with classical hydrothermal synthesis and homogenous temperature fields inside the vessels.^[19] The generation of a solid Ir-compound via MW-assisted hydrothermal synthesis is determined by the complex chemistry of solvated Ir-species under basic conditions and high temperatures. With regards to desired high synthesis yields, the reduction of Ir^{IV}-iridates to Ir^{III}-iridates in high pH media via the oxidation of OH⁻ (Scheme 1) is a key mechanism.^[20]



Scheme 1. Reduction of hexachloroiridate-(IV) to hexachloroiridate-(III) in basic media

The reduction to Ir^{III}-iridates is a crucial step as these species are prone to hydrolysis via Scheme 2, whereas Ir^{IV}-iridates are stable in solution upon heating and result in lower yields of solid product. Upon addition of base to the Ir^{IV}-solution strong decoloring of the solution is observed, which corresponds to the disappearance of strong ligand-to-metal charge transfer bands following the reduction of the Ir^{IV}-chloride complex to the 5d⁶-Ir^{III}-complex.^[20]



Scheme 2. Hydrolysis of hexachloroiridate-(III) in basic media

Furthermore, the pH has also been suspected to strongly influence the oligomerization and condensation processes of the hydrolyzed Ir-species.^[21,22] Accordingly, in order to investigate the influence of the initial KOH:Ir-ratio, a series of seven Ir-based catalysts were produced via MW-assisted hydrothermal treatment at 250°C, from precursor solutions containing varying initial molar KOH:Ir-ratios from 1:1 to 100:1 (1:1, 4:1, 5:1, 7:1, 10:1, 50:1, 100:1) while maintaining the total Ir-concentration at 10⁻² mol L⁻¹. Fig. S1 shows the relevant synthesis parameters monitored during the MW-synthesis. It shows that when held at 250°C for 1h, the pressure inside the reaction vessels steadily increased, which is due to the gas liberation from water decomposition via Scheme 1. For better overview, for each samples the relevant synthesis parameters and characterization data are listed in Table S1.

UV-Vis. — Ultraviolet visible spectroscopy (UV-Vis) analysis of the supernatant resulting from hydrothermal MW-treatment and the first centrifugation allows for the detection of residual solvated Ir-species and insight into the mechanisms involved in the condensation of the solid product (Fig. 1). In the case of low initial KOH:Ir-ratios (≤4:1), the UV-Vis spectra reveal two weak absorption bands at 321 nm and 380 nm which are attributed to partially hydrolyzed Ir^{III}-chloride complexes^[23,24]. These partially chlorinated species still exhibit strong stability against hydrolysis upon heating, which explains the low yield of 51% observed for

KOH:Ir=1:1. Yields were calculated using molar masses extracted from the gathered compositional information (see Table S1 in S.I). Conversely, with a large excess of KOH, *i.e.*, KOH:Ir≥7:1, stable Ir(OH)₆³⁻ species identified by a strong absorption band at 313 nm were identified in the supernatant, also decreasing the final synthesis yield.^[25] The prevalence of Ir-monomers at high pH has been attributed by Gamsjäger et al. to fast hydroxyl-ligand exchange kinetics hindering oligomerization and condensation of hydrolyzed Ir-species.^[21,26] In the intermediate KOH:Ir regime (4:1≤KOH:Ir≤7:1) only weak absorption features, were observed which corresponds to the formation of oligomeric Ir-species resulting in a high synthesis yield (≥97%).^[21]

It appears that the KOH:Ir-ratio is a crucial parameter in optimizing the synthesis yield of rare-earth Ir-compounds produced via hydrolyzation of hydrolyzed Ir-species. Concerning the impact of the KOH:Ir-ratio on the nature of the produced compounds, it should be noted at this point that most authors emphasize possible re-oxidation of Ir^{III}- to Ir^{IV}-species by dissolved oxygen. Oligomerization and condensation reactions are thus in competition with re-oxidation, leading to a wide range of possible products. Under basic conditions, authors have suggested the formation of binuclear oxo-bridged mixed-oxidation Ir-complexes^[27] and even peroxy-bridged Ir^{III/IV}-oligomers^[28]. The wide array of proposed products highlights the complexity of the oligomerization chemistry of hydrolyzed Ir-species and suggests great precaution when analyzing the composition of resulting products.

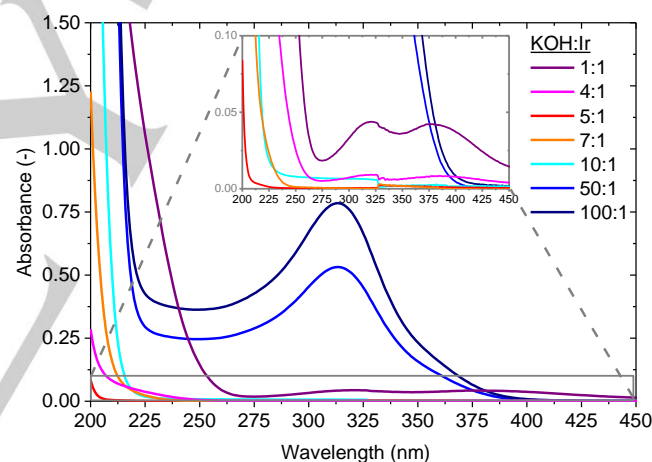


Figure 1. Absorption spectra measured by UV-Vis spectroscopy of Ir-species remaining in solution after MW-assisted hydrothermal synthesis. The insert shows a magnification in the 200 to 450 nm region necessary for a better observation of weaker bands. The KOH:Ir ratios is given in the figure legend.

XRF. — X-ray fluorescence spectroscopy was used in order to assess elements present in the solid Ir-compounds after washing and drying. For low KOH:Ir-ratios, significant amounts of Cl relative to Ir were detected for KOH:Ir ≤ 4:1 (Table S1). The presence of chlorides for the low KOH:Ir-ratios is in line with the partial hydrolyzation of Ir-chloride precursors indicated by the presence of chlorinated species in solution after MW-treatment (inset in Fig. 1). No traces of Cl were detected for higher KOH:Ir-ratios, confirming the complete hydrolyzation of Ir-precursors for KOH:Ir≥5:1. These results support the efficient formation of a Cl-free oligomeric Ir-species at intermediate KOH:Ir-ratios (≥ 4:1 to ≤10:1). Thus the MW-assisted hydrothermal synthesis methodology contrasts with most previous studies where Ir-oxides prepared from Ir-chloride precursors retain significant amounts of Cl-impurities.^[29–32]

Additionally, XRF-results showed significant variations in the relative amount of K to Ir found in the samples (Fig. 2.b). The K-

content was found to be relatively low for KOH:Ir=5:1, while significantly increasing for KOH:Ir \geq 7:1. Although the amount of base only doubled between KOH:Ir= 5:1 and KOH:Ir=10:1, the amount of incorporated K was over six times higher for KOH:Ir=10:1. This sharp increase in K-uptake is indicative of a change in the way the Ir-structures incorporate K for KOH:Ir \geq 7:1. In order to investigate such structural variations, powder x-ray diffraction (P-XRD) was employed.

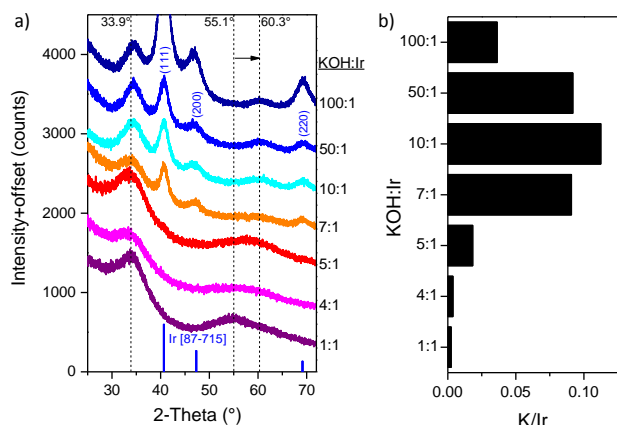


Figure 2.a) Powder X-ray diffraction patterns of Ir-based catalyst synthesized for various KOH:Ir-ratios in the region $25^\circ \leq 2\theta \leq 72^\circ$. The reference pattern of metallic Ir⁰ is shown blue bars (PDF [87-715]); **2.b)** shows the corresponding K/Ir-ratio determined via XRF for each sample. See Table S1 for the error evaluation of the KOH:Ir measurements.

XRD.— All MW-produced samples exhibited two broad diffraction features centered at $2\theta = 33.9^\circ$ and $55.1^\circ \leq 2\theta \leq 60.3^\circ$ (dashed lines in Fig. 2.a, Fig. S2). Such a pattern is distinct both from the rutile-type pattern of IrO₂ and from the hollandite-type pattern of K_{0.25}IrO₂. Indeed, for both IrO₂ and K_{0.25}IrO₂ a strong diffraction feature would be expected at $2\theta = 28^\circ$ (Fig. S2). Broad features at similar 2θ -values have previously been reported for electrochemically grown amorphous Ir-oxohydroxides.^[33,34] As a result, the two broad features are a first indication of the successful formation of the desired Ir-oxohydroxide phase. The appearance of two diffraction features indicates the presence of a nanocrystalline Ir-phase, rather than a completely amorphous structure. Even though the broadness of the features didn't allow for any reliable structural analysis, a clear shift of the second peak from $2\theta = 55.1^\circ$ to $2\theta = 60.3^\circ$ was observed with increasing KOH:Ir-ratios (Fig. 2.a). It is not clear whether this shift is the sign of a gradually decreasing interplanar distance in the nanocrystalline arrangement of the Ir-structure with increasing KOH:Ir or a concomitant appearance of a diffraction feature at $2\theta = 60.3^\circ$ and the disappearance of a feature at $2\theta = 55.1^\circ$ is also possible.

XRF also showed that the total K-content was not continuously growing with KOH:Ir. For KOH:Ir \geq 50:1, the K-content seemed to be decreasing again. The observed decrease is due to the increasing formation of metallic Ir⁰ at higher KOH:Ir, as revealed by XRD for KOH:Ir \geq 7:1 (blue bars and indexed peaks in Fig. 2.a and Fig. S2). The increasing formation of Ir⁰ under more alkaline conditions is attributed to the reduction of Ir^{III}-species to Ir⁰ via the oxidation of hydroxyl anions under MW-treatment conditions. The metallic Ir⁰ is unlikely to accommodate K, as indicated by the good agreement between the indexed diffraction peaks with the reference pattern (Fig. 2.a and Fig. S2). As a result, since XRF only allows to assess the overall K-content, the growing K-free Ir⁰-phase explains the levelling and subsequent decrease of K-contents with rising KOH:Ir. The broad XRD-feature remains however centered around $2\theta = 60.3^\circ$ for KOH:Ir \geq 10:1, showing

that the structural change induced by K was stable. This is an indication that the K-content of the suspected nanocrystalline Ir-oxohydroxide phase remains stable for KOH:Ir \geq 10:1.

The two commercial Ir-reference compounds SA-IrO₂ and AA-IrO_x were described in detail by Pfeifer et al. and used to demonstrate the superior electrochemical properties of Ir-oxohydroxides.^[16] Briefly, SA-IrO₂ is a crystalline rutile IrO₂ (Fig. S3.a), while AA-IrO_x was characterized by Pfeifer et al. as a quasi-amorphous Ir-oxohydroxide. In addition to a metallic Ir⁰-impurity, the XRD-pattern of AA-IrO_x exhibits two broad diffraction features at $2\theta = 34.1^\circ$ to $2\theta = 58.1^\circ$ (Fig. S3.b), similar to what was observed for the present MW-produced Ir-compounds. This observation is an additional indication that the two broad features observed around $2\theta = 34^\circ$ and $55.1^\circ \leq 2\theta \leq 60.3^\circ$ are characteristic of quasi-amorphous, nanocrystalline Ir-oxohydroxide structures.

SEM/BET.— In order to gain insight into sample morphology and structure, scanning electron microscopy (SEM) and specific surface area (S_{BET}) analysis of the compounds were used. For the Cl-containing samples produced at low ratio of KOH:Ir \leq 4:1, SEM-images reveal a nanostructured morphology (Fig. S4) in line with a high S_{BET} over $150 \text{ m}^2 \text{ g}^{-1}$ (Table S1). At elevated ratios of KOH:Ir \geq 50:1, the compounds are composed of compact 200 nm spheres, in agreement with the observed sharp decrease in surface area to 7 and $16 \text{ m}^2 \text{ g}^{-1}$ respectively for KOH:Ir=50:1 and 100:1 (Fig. S4).

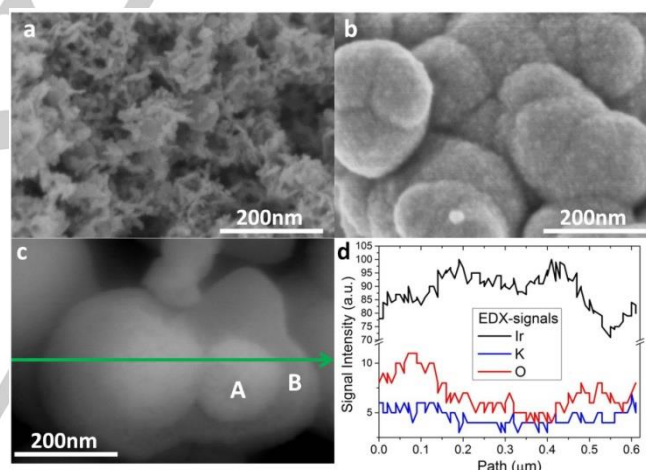


Figure 3. SEM of the nanostructured compound synthesized for KOH:Ir = 5:1 (a) shows a highly nanostructured material, whereas for a ratio of KOH:Ir = 50:1 (b) more compact clusters are formed. Secondary electron contrasted-imaging (YAG-BSE detector) of such a split cluster (c) reveals a core-shell structure, where the metallic iridium (bright twin-cores, A) is coated with a thick layer of oxidic iridium (B). d) Linescan (following the green arrow in 3c) confirms lower O:Ir-ratio in the Ir⁰-cores.

The sample produced at KOH:Ir=50:1 was analyzed further in-depth and the study of some cracked open spheres revealed a core-shell structure (Fig. S5). The Ir-core was identified as metallic Ir⁰ coated with a thick oxidic Ir-layer (over 50 nm) using atomic number sensitive secondary electron contrasted imagery (Fig. 3.c and Fig. S5). An EDX-linescan through such a split core-shell-cluster reveals lower O:Ir-ratios within the metallic Ir-core (Fig. 3.d). The core-shell structure revealed by SEM for KOH:Ir=50:1 suggests that the Ir⁰ detected in XRD for higher KOH:Ir-ratios is present within a core-shell structure below an oxidic Ir-layer. During MW-treatment such Ir-cores are probably formed for high KOH:Ir-ratios during an initial stage by the reduction of Ir^{III}-species in presence of high OH⁻-concentrations via hydroxyl oxidation. The Ir⁰-cores then serve as nucleation sites for the oxidic layer formed on top once the OH⁻

concentration decreases. Further in-situ analysis during MW-treatment will be needed to confirm this interpretation. Most importantly this analysis reveals that the metallic Ir⁰ detected in some samples via XRD is located under a thick oxidic Ir-layer and should thus not contribute to the electrochemical properties of the produced material.

For intermediate ratios, $5:1 \leq \text{KOH}:\text{Ir} \leq 7:1$, where Ir-compounds were formed at high synthesis yields, a nanosized rod-type structure is obtained (Fig. 3a and Fig. S4). Particle thickness increases with KOH:Ir, while S_{BET} decreases from 104 to $56 \text{ m}^2 \text{ g}^{-1}$. For KOH:Ir=10:1, S_{BET} suddenly increased to $175 \text{ m}^2 \text{ g}^{-1}$ while an undefined structure was observed in SEM. The sudden change in BET surface area, for the sample KOH:Ir=10:1, is not yet understood. However, it may be related to two different nucleation and growth mechanisms. In the lower KOH:Ir-ranges, oxidic Ir forms as nanostructured rod-shapes, whereas at higher KOH:Ir, Ir⁰-cores form.

STEM.— In order to gain more in-depth knowledge about the nanocrystalline oxidic Ir-phase, the Ir⁰-free sample prepared from KOH:Ir=5:1 was investigated in scanning transmission electron microscopy (STEM). Energy-dispersive x-ray analysis (EDX)-mapping revealed homogenous Ir- and O-contents, as well as K and low Cl-traces (Fig. S6). However, no reliable structural information about the crystallographic nature of the oxidic Ir-phase could be retrieved as at higher magnification the sample rapidly transformed into crystalline metallic Ir⁰ under the electron beam. Fig. 4 shows the beam damage observed for a $15 \mu\text{A}$ -STEM electron beam over 213 s. Even the initial picture already shows bright spots corresponding to metallic Ir. These spots served as nucleation sites for rapidly expanding Ir⁰-nanoparticles revealed by the growing bright particles at 33 s and 213 s.

Thus, the STEM-study emphasizes the difficulty to characterize quasi-amorphous oxidic Ir-phases via TEM-imagery^[32], which contrasts with crystalline IrO₂ which can be studied under similar electronic illumination conditions without major beam damage^[35].

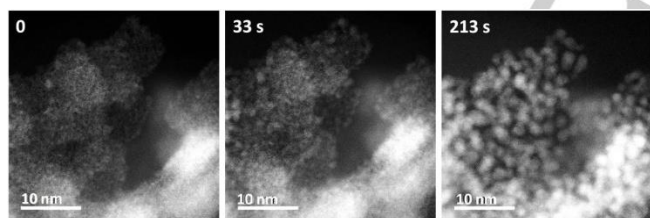


Figure 4. Time-resolved STEM imaging of the Ir-compound obtained from KOH:Ir=5:1 using a $15 \mu\text{A}$ -electron beam. Pictures were taken initially, after 33 s and after 213 s (from left to right).

TGA-MS.— In order to determine the composition of the MW-produced Ir-compounds, especially the extent of hydroxylation, the sample decomposition to crystalline IrO₂ and simultaneous water release were analyzed via thermogravimetric analysis (TGA). The observed mass changes coupled to the analysis of evolved gas using mass spectrometry (MS) yield relevant information on sample composition and chemical nature of functional groups as shown by Bestaoui et al for Ir-oxohydroxide type structures.^[36] Upon heating at 10 K min^{-1} from room temperature (RT) to $800 \text{ }^\circ\text{C}$ in a 21%-O₂/Ar flow (100 mL min^{-1}), the samples exhibited a first weight loss (below $150 \text{ }^\circ\text{C}$) related to the removal of physisorbed water, denoted $\phi\text{-H}_2\text{O}$ (Fig. 5 and Fig. S7). Water evolution then proceeds further until $500 \text{ }^\circ\text{C}$ and accounts for up to 7 wt.% of the total initial sample mass for KOH:Ir=5:1. Water evolution above $150 \text{ }^\circ\text{C}$ for oxidic Ir-compounds was attributed to hydroxyl decomposition.^[16,36] Taking into account the high relative mass of Ir, several wt.% of water lost through hydroxyl decomposition indicates a high

degree of hydroxylation. IrO₂ on the other hand has been reported to loose negligible amounts of water during TGA-MS.^[16] The water fraction removed through hydroxyl decomposition was highest for the samples synthesized for KOH:Ir $\leq 5:1$ (ca. 6-7 wt.%) and gradually decreased with higher KOH:Ir (Table S1). Based on the elevated hydroxyl weight fractions, the composition of the oxidic phase of the MW-produced electrocatalysts is an Ir-oxohydroxide of the general form IrO_x(OH)_y.

Interestingly, in addition to their elevated hydroxylation level, samples with KOH:Ir $\leq 5:1$ exhibited a strong component in their water evolution signal above $300 \text{ }^\circ\text{C}$ (Fig. 5 and Fig. S8). Higher decomposition temperatures are indicative of the distinct chemical nature of hydroxyl groups present in these compounds. In-situ investigation of the hydroxyl decomposition based on diffuse reflectance IR-spectroscopy (DRIFTS) was attempted in order to assign spectroscopic signatures to the various hydroxyl groups (not shown). The measurements were unsuccessful due to the highly reflective properties of Ir-oxides^[37] and the low quality of resulting spectra. However, based on the water evolution signals observed during TGA-MS, it can be pointed out that the samples prepared for lower KOH:Ir-ratios feature a higher amount of hydroxyl groups decomposed at higher temperatures. The presence of such particular hydroxyl groups can be of interest when discussing the OER-properties of Ir-oxohydroxides.^[15]

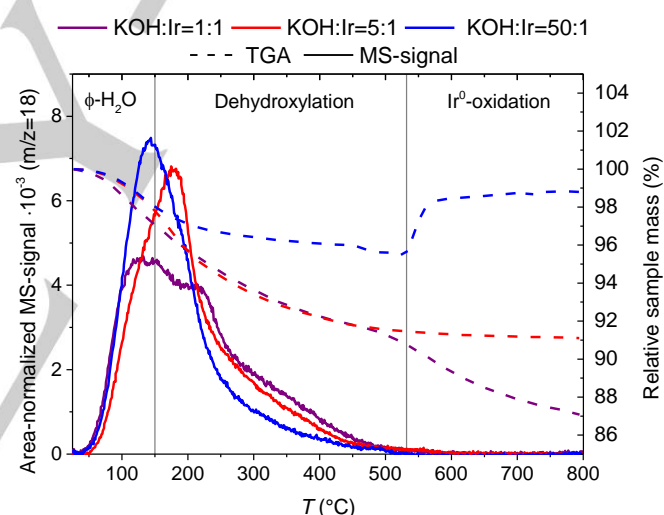


Figure 5. TGA of three representative Ir-compounds (KOH:Ir=1:1, 5:1 and 100:1) decomposition in 21% O₂/Ar (100 mL min^{-1}) with MS-analysis of evolved gas (detailed curves in S.I. Fig. S7 and S8).

The amount of metallic Ir⁰ present for higher KOH:Ir-ratios was estimated from the sharp mass gain associated with a strong exothermal heat signal detected above $500 \text{ }^\circ\text{C}$ for KOH:Ir $\geq 7:1$ (Fig. S7). This event corresponds to the oxidation of Ir⁰ to Ir^{IV}. XRD of the samples after TGA-MS confirms the total oxidation (Fig. S9). It appears that the Ir⁰-fraction increases gradually with increasing KOH:Ir, reaching 24 mol.% for KOH:Ir=50:1 (calculation in S.I., p. 9), which is in agreement with the evolution of Ir⁰-patterns observed in XRD (Fig. 2). The gradual increase of the Ir⁰-fraction with KOH:Ir confirms the hypothesis that at higher initial pH, Ir^{III}-species are reduced to Ir⁰ under MW-treatment conditions. Ir^{III}-reduction through hydroxyl decomposition is likely, however a disproportionation mechanism cannot be excluded either. It should also be noted that above $500 \text{ }^\circ\text{C}$, the Cl-containing samples featured a pronounced mass decrease (KOH:Ir=1:1 in Fig. 5), which corresponds to Cl₂-evolution.

TPR.— The reduction behavior of the samples was studied in a temperature-programmed reduction (TPR) experiment using a 4.92%–H₂/Ar stream (80 mL min⁻¹). Upon heating the samples to 300 °C, sharp reduction features were observed between 60 °C and 100 °C for the catalysts synthesized for KOH:Ir ≤ 7:1. For comparison purposes, Fig. 6 also shows the TPR-signals obtained for AA-IrO_x (green profile) and SA-IrO₂ (black profile). AA-IrO_x exhibited a sharp reduction feature at 73°C, similar to what was observed for the MW-produced compounds. The reduction behavior observed for Ir-oxohydroxides was thus clearly distinct from the broad reduction feature of crystalline SA-IrO₂ centered at 239°C, in agreement with literature values for IrO₂-reduction.^[14] Sharp reduction features below 100°C seem to be characteristic of quasi-amorphous Ir-oxohydroxides as noted by Reier et al. who used such TPR-profiles to distinguish their compounds from crystalline IrO₂.^[14]

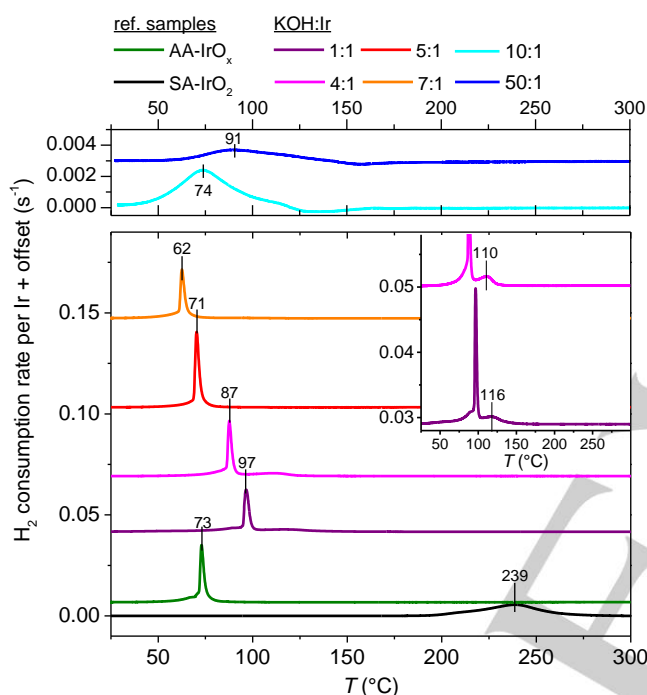


Figure 6. TPR measured at 6 K min⁻¹ in 4.92 vol.% H₂/Ar. The measurements show sharp reduction features below 100 °C for the MW-produced Ir-samples as well as AA-IrO_x (dark line) in contrast to the characteristic reduction feature of IrO₂ found above 200 °C, as observed with the reference compound SA-IrO₂ (green line).

Furthermore, the comparison of TPR-profiles showed a gradual shift to lower temperatures from 97°C (KOH:Ir = 1:1) to 62°C (KOH:Ir = 7:1). The trend was inverted for higher KOH:Ir-ratios (KOH:Ir ≥ 10:1), where the TPR-profiles broadened significantly and shifted again towards higher temperatures. This upward shift of the characteristic reduction peak is likely related to the changes in sample morphology observed via SEM (Fig. 3 and Fig. S4) with the formation of more compact structures at higher KOH:Ir-ratios. We also suggest that the observed reduction temperature trend is linked to the evolution of the K-content in the samples (Fig. 2.b). For KOH:Ir ≤ 7:1, the downward shift of reduction temperatures is in line with the increasing K-content of the nanocrystalline Ir-oxohydroxide phase. This evolution is an indication that the presence of K in the structure influences the reducibility of Ir-oxohydroxides, which is likely to affect the redox properties of the compounds.

Additional shoulders in the reduction peaks for KOH:Ir = 1:1 and 4:1, respectively at 116°C and 110°C (inset in Fig. 6) were

attributed to the presence of chlorides in the sample, which influence the reduction mechanism.

In addition, it is noteworthy that a significant amount of H₂ was consumed by Ir-oxohydroxides at RT (Table S1) without detectable evolution of water (Fig. S10) according to MS. This observation is in line with the results reported by Reier et al. who reported RT-H₂-uptake for Ir-oxohydroxides during TPR.^[14] The absence of RT-H₂-consumption for the crystalline SA-IrO₂ supports the hypothesis that significant RT-H₂-uptake is characteristic of Ir-oxohydroxides as opposed to crystalline IrO₂. The absence of water evolution indicates that H₂ is most likely strongly adsorbed onto the samples at RT. Since no subsequent H₂-release is observed, the adsorbed H₂ must participate in sample reduction upon TPR and has to be taken into account when determining the total H₂-consumption. Overall, the high reducibility of Ir-oxohydroxides and their affinity for nucleophilic species such as H₂ at RT sets them apart from crystalline IrO₂ characterized by relative inertness under reducing conditions at temperatures below 200°C.

Catalyst composition and averaged oxidation state.— The nominal sample composition and average Ir-oxidation state were estimated based on the total H₂-consumption during TPR, TGA-MS and elemental ratios determined via XRF (see p. 9 in S.I.). The calculations show a gradual increase of the average Ir-oxidation state from +3.2 to +3.7 for KOH:Ir-ratios varying from 1:1 to 50:1. The contribution from the metallic Ir-phase has been extracted from these results based on the Ir⁰-fraction determined via TGA-MS so that the average oxidation state corresponds solely to the oxidic Ir-phase. The observed increase of the Ir-oxidation state towards +4 for higher KOH:Ir-ratios is in agreement with the observed shift of characteristic TPR-features towards higher temperatures (Fig. 6). Moreover, the obtained values suggest the presence of mixed Ir-oxidation states, namely Ir^{III} and Ir^{IV}, in keeping with recent findings on the electronic structure of quasi-amorphous Ir-oxohydroxide compounds backed by ab-initio calculations and X-ray photoemission studies.^[16,17] In these studies, the AA-IrO_x benchmark reported in the present TPR-experiment was investigated and characterized as an Ir^{III/IV}-oxohydroxide.^[16] The similar characteristics of the MW-produced samples described via XRD, TGA-MS and TPR supports the hypothesis that their oxidic phase also consists of an Ir^{III/IV}-oxohydroxide.

The determination of the average Ir-oxidation state also allowed for the quantification of the hydroxyl fraction decomposed between 150 and 550°C (Fig. 5, Table S1). The results confirm that the OH-fraction in the samples was highest at lower KOH:Ir-ratios and diminishes with increasing KOH:Ir. For the essentially Cl-free and Ir⁰-free Ir-oxohydroxide obtained for KOH:Ir = 5:1, a nominal composition of IrO_{0.9}(OH)_{1.8} was obtained. The important hydroxyl fraction confirms that hydroxyl groups are not simply formed as surface groups but are part of the compound lattice, confirming the successful formation of bulk Ir-oxohydroxides. In order to link the observed variations in catalyst composition to the resulting electrocatalytic properties, the following step was to determine the compounds' OER-performance.

Electrocatalytic OER-activity.— The OER-activity of the samples was evaluated based on the overpotential needed to reach a current density (*j*) of 10 mA cm⁻² ($\eta_{j=10 \text{ mA cm}^{-2}}$) during linear sweep voltammetry (LSV) in H₂SO₄ (0.5 mol L⁻¹). This activity-indicator is a widely accepted figure of merit.^[4,38] Electrode loadings of 20 μg_{Ir} cm⁻² were used, which is two orders of magnitude lower than current literature standards.^[2] This method provides a robust and primary figure of merit for the comparison of OER-activities within the produced series of Ir-oxohydroxides. The MW-produced compounds are also compared to the two

commercial benchmarks AA-IrO_x and SA-IrO₂, which have been extensively characterized by Pfeifer et al.^[16]

The overpotentials are listed in Fig.7 (red bars, full LSV in Fig. S12). It appears that the lowest overpotentials were observed for the Ir-oxohydroxides produced for KOH:Ir ≤ 7:1, i.e. the samples containing no or little traces of Ir⁰. Chlorine evolution can be excluded for KOH:Ir≥5:1, as the samples were essentially Cl-free according to XRF. For higher KOH:Ir-ratios, overpotentials gradually increase, showing a decrease in OER-activity of the samples. Interestingly even the least active MW-produced Ir-oxohydroxide obtained for KOH:Ir = 100:1 was more active than the commercial AA-IrO_x Ir-oxohydroxide. The crystalline SA-IrO₂ didn't reach $j=10$ mA cm⁻² within the set potential window. These results are a first corroboration of the crucial role played by the KOH:Ir-ratio synthesis parameter in tuning OER-relevant sample properties. Note that Tafel plots were not generated as the kinetic interpretation of the results proves to be delicate for a process involving multiple electron transfers.^[3, 39,40]

Morphological effects could be excluded as no correlation with S_{BET} was found. For instance the sample produced for KOH:Ir = 10:1 required higher overpotentials to reach $j=10$ mA cm⁻² than the sample produced for KOH:Ir = 7:1, despite S_{BET} of respectively 175 and 56 m².g⁻¹. The results indicate that the OER-activity is dominated by the intrinsic activity of the compounds, which is determined by the synthesis parameters of our MW-assisted hydrothermal synthesis.

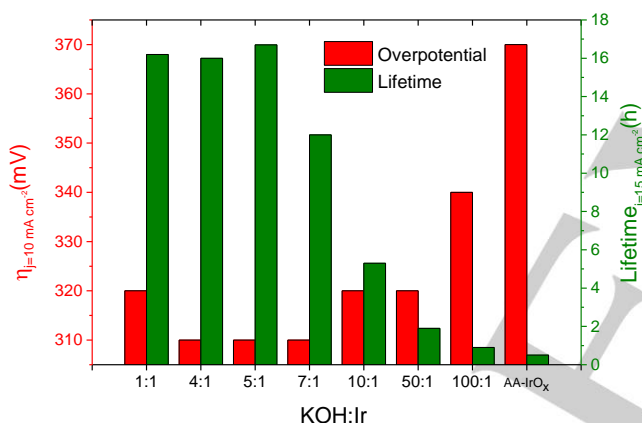


Figure 7. OER-activity (red bars) and OER-stability (lifetime at $j=15$ mA cm⁻²) of Ir-oxohydroxides produced via MW-assisted hydrothermal synthesis and commercial benchmark AA-IrO_x.

Electrocatalytic OER stability.— In order to assess OER-stability, the catalyst lifetime during a chronopotentiometric (CP)-experiment at $j=15$ mA cm⁻² was used as a stability indicator. The lifetime was defined as the time-lapse required by the working electrode to reach a threshold potential of 1.8 V vs. SHE. Such a threshold corresponds to the onset of the glassy carbon (GC) support corrosion.^[41] The current density of $j=15$ mA cm⁻² was chosen as accelerated testing conditions. The reproducibility of the results was verified in two different acidic electrolytes, H₂SO₄ (0.5 mol L⁻¹) and HClO₄ (0.5 mol L⁻¹) and showed no significant difference except for various noise levels assigned to variations in bubble removal efficiency due to irregularities on the prepared electrode surface (Fig. S14).

Besides crystalline SA-IrO₂, which was immediately deactivated, all samples could maintain $j=15$ mA cm⁻² in the hour-range (CP-curves in Fig. S13). Typically CP-curves exhibit a long time-range of gradually growing overpotentials in the range of 1.55-1.65 V vs. SHE. The slow increase is indicative of a progressive deactivation mechanism of the electrocatalysts. Once a threshold of ca. 1.65 V vs. SHE has been reached,

overpotentials increase dramatically fast, indicating a different deactivation mechanism. Cherevko et al. have reported the onset of corrosive Ir-dissolution for Ir-oxide anodes at potentials above 1.65V vs. SHE, which explains the observed fast deactivation at higher anode potentials.^[42] It can however be excluded that a significant part of the observed currents are due to non-faradaic electrode processes such as Ir-corrosion. Indeed the anodic charge obtained during the hour-long CP-experiments for the MW-produced compounds is three to five orders of magnitude above the charge that could theoretically be obtained from the oxidation of all the Ir deposited on the anode. Nonetheless the different deactivation behaviors emphasize the relevance of the potential range in which the catalysts are operated. A more in-depth in-situ study will have to determine the exact deactivation mechanism in the potential range below ca. 1.65 V vs. SHE in order to define strategies to prevent Ir-based OER-catalysts from reaching corrosion-potentials.

The samples synthesized for KOH:Ir ≤ 5:1 exhibited comparable lifetimes with a maximum of 16.7 hours for the Ir-oxohydroxide synthesized from KOH:Ir=5:1, indicating similar OER-stabilities. The catalyst OER-stability decreased substantially for higher KOH:Ir ratios and reached a minimum of 30 minutes for AA-IrO_x used as benchmark, corresponding to ca. 33 times shorter lifetime than the MW-sample obtained for KOH:Ir=5:1. Based on its optimal OER-performance, the Ir-oxohydroxide synthesized at a ratio of KOH:Ir=5:1 was selected as the target material, due to the high synthesis yield and the high purity with regards to Ir⁰ and Cl. The selected compound was further tested in CP at 10 mA cm⁻² for comparison with recent benchmarking efforts by McCrory et al (see Table 1 and CP in Fig. S15).^[4,38] The comparison to the results of McCrory et al. was shown due to the similar testing conditions used (electrolyte, RDE, temperature). Otherwise comparisons often result in an apple and orange-like situation due to the large variety of testing conditions used throughout the literature.

Table 1. Benchmarking parameters for the best MW-compound (KOH:Ir=5:1) compared to the AA-IrO_x benchmark and to previously reported benchmarks.

Catalyst	$\eta_{j=0}$ (V)	$\eta_{j=2h}$ (V)	$\eta_{j=24h}$ (V)	Metal loading ($\mu\text{g cm}^{-2}$)	H ₂ SO ₄ -electrolyte (mol L ⁻¹)
KOH:Ir=5:1	0.31	0.33	0.35	20	0.5
KOH:Ir=5:1	0.31	0.33	0.35	50	0.5
KOH:Ir=5:1	0.30	0.32	0.33	100	0.5
AA-IrO _x	0.37	— ^[b]	— ^[b]	20	0.5
SIROF ^[4]	0.34	0.36	0.44	n.r. ^[a]	1
Sputtered Ru ^[4]	0.28	0.34	0.82	n.r. ^[a]	1

[a] Reactive sputtering resulted in a >100nm thick films (see ref.[4,43]); [b] AA-IrO_x was active for only 62 min.

For Ir-loadings as low as 20 $\mu\text{g Ir cm}^{-2}$, the best MW-produced catalyst surpassed the best benchmarks reported by McCrory et al. in terms of evolution of the overpotential needed to maintain $j=10$ mA cm⁻² (Table 1). Such performance constitutes a significant improvement as Ir-loadings reported in the literature are usually two orders of magnitude higher when stability on the hour-scale is to be achieved at relevant current densities.^[2] Interestingly, for Ir-loadings of 100 $\mu\text{g Ir cm}^{-2}$, a lifetime of 48 h was obtained. The increase of lifetime with higher loadings is an indication that the deactivation mechanism below 1.65 V vs. SHE is less potential dependent rather than turnover-dependent. At the same current density for higher catalyst loadings and more exposed active sites, each site processes less OER-reactions. The improved lifetime is an indication that deactivation of Ir-oxohydroxide-based OER-catalysts below 1.65 V vs. SHE can be linked to side-reactions inhibiting OER-active sites.

The OER-performance of the MW-produced Ir-oxohydroxides confirms the clear superiority of nanocrystalline Ir-oxohydroxides over their crystalline IrO₂-counterparts. In addition, the high disparity of OER-performances obtained for varying KOH:Ir-ratios highlights the relevance of MW-synthesis conditions.

In a last step, correlations between OER-performance and structural features of the MW-produced Ir-oxohydroxides were investigated in order to identify OER-relevant characteristics. For this purpose we used the current density obtained at $\eta=0.35$ V during LSV ($j_{\eta=0.35V}$) which is a commonly used metric for a robust assessment of OER-activity.^[4] Several recent literature reports have highlighted the relevance of the hydroxylation level of high-performance Ir^{III/IV}-electrocatalysts.^[15,16,35] The authors emphasized the possible link between high OER-performance of quasi-amorphous Ir-electrocatalysts and the presence of reactive hydroxyl groups in a mixed oxidation state Ir-environment. In order to investigate a possible link between OER-performance and hydroxylation level of Ir-oxohydroxides, we compared $j_{\eta=0.35V}$ to the wt.% of chemisorbed water evolved during TGA-MS, via dehydroxylation (Fig. 8).

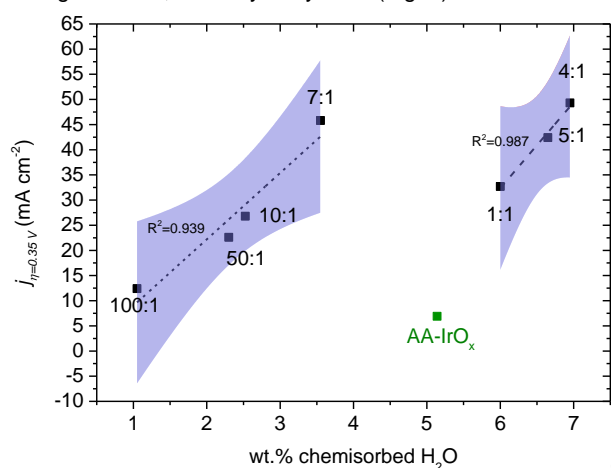


Figure 8. Current densities obtained at $\eta=0.35$ V during LSV as a function of the wt.% of water removed through decomposition of hydroxyl groups (chemisorbed water) during TGA-MS for the MW-produced Ir-oxohydroxides (black squares with KOH:Ir-ratios indicated next to them) and the commercial benchmark AA-IrO_x (green square). The dashed lines are linear fits (first order polynomial) of the two groups of data points corresponding to the MW-samples and their corresponding 95% confidence interval (light blue area).

Within the MW-produced compound family, two groups of data points were evidenced: For both the samples produced for KOH:Ir ≤ 5:1 and for KOH:Ir ≥ 7:1 a linear trend was observed (dashed lines in Fig. 8). These trends show for both groups that higher hydroxylation levels match with higher $j_{\eta=0.35V}$. The samples prepared for KOH:Ir ≤ 5:1, which exhibited the highest chemisorbed water fractions (6-7 wt.%) also exhibited some of the highest current densities. On the contrary, the samples produced for KOH:Ir ≥ 10:1, with chemisorbed water fractions below 3 wt.% exhibited significantly lower current densities. The sample produced for KOH:Ir = 7:1 constitutes an outlier as despite a chemisorbed water fractions of only 3.6 wt.%, it equals the current densities of the best samples. The AA-IrO_x benchmark on the other hand contained a chemisorbed water fraction of 5.1 wt.% but presented with the lowest $j_{\eta=0.35V}$ -value. These divergent behaviors indicate that the OER-performance of Ir-oxohydroxides cannot be assessed simply based on the level of hydroxylation of the sample.

A conclusive identification of OER-relevant hydroxyls is challenged by the difficulty of distinguishing the different types of hydroxyl groups and factors influencing their reactivity. Pfeifer et al. showed that in the case of X-ray photoelectron spectroscopy (XPS), assignments of O1s contributions to hydroxyl groups need to take into account the particular electronic structure of Ir-oxides and cannot be undertaken solely based on binding energy shifts.^[16] Nonetheless, the observed trends linking higher OER-performance to higher hydroxylation levels of Ir-

oxohydroxides are consistent with the presence of OER-relevant Ir-OH-species in Ir-oxohydroxides suggested in previous studies.^[15,35]

Moreover, the falling of the MW-produced Ir-oxohydroxides into two different groups (Fig. 8) compares with the structural properties of the compounds described in the previous sections. The best OER-catalysts prepared for KOH:Ir ≤ 5:1 were characterized by high hydroxyl fractions, low K-content (Fig. 2.b) and sharp reduction features in TPR (Fig. 6). The sample prepared at KOH:Ir = 7:1 still presented a sharp TPR-peak (Fig. 6) and low overpotentials (Fig. 7), it however contained significantly more K, a much lower hydroxyl fraction and had a reduced lifetime at $j=15$ mA cm⁻². This compound thus illustrates the structural transition towards a K-rich Ir-oxohydroxide phase with rising KOH:Ir. In such a K-rich Ir-oxohydroxide the OER-activity is still linked to the hydroxyl fraction (Fig. 8), but exhibits much lower stability (Fig. 7). This suggests that high K-contents are detrimental to the OER-performance of Ir-oxohydroxides in that they lead to the formation of a distinct Ir-oxohydroxide phase characterized by an XRD-peak at approx. 60.3° (Fig. 2.a) and less stable under OER-conditions. It should be noted that the observed trends in OER-performance did not correlate with the specific surface area of the compounds. Morphological factors might still play a significant role but seem to be dominated by the intrinsic OER-performance of the obtained Ir-oxohydroxide phases.

The diminishing OER-performance of K-rich Ir-oxohydroxides suggests an adverse effect of high K-contents. However the results obtained for AA-IrO_x, which contains no K at all, suggest that a completely K-free Ir-oxohydroxide phase is not desirable either. Indeed, although the structure of AA-IrO_x was found to be close to the best electrocatalysts obtained for KOH:Ir ≤ 5:1, it exhibited by far the worst OER-performance. The only feature setting AA-IrO_x apart is the complete absence of K from the compound. Otherwise, AA-IrO_x exhibits an intermediate hydroxyl fraction (Fig. 8) as well as a sharp TPR reduction peak (Fig. 6) and RT-H₂-uptake (Table S1) similar to the Ir-oxohydroxide obtained for KOH:Ir = 5:1. Morphological effects cannot account for the poor OER-performance of AA-IrO_x, as with $S_{BET}=33$ m²g⁻¹ it is only three times lower than for KOH:Ir = 5:1. It follows that the absence of K has a dramatic effect on the OER-performance of Ir-oxohydroxides limiting both their OER-activity and stability. Low K-contents as found in the compounds obtained for KOH:Ir ≤ 5:1 seem to constitute an optimum, enhancing both the activity and the stability of Ir-oxohydroxide electrocatalysts under acidic OER-conditions.

The OER-relevance of cations such as K⁺ has been pointed out recently by Gao et al.^[44] The authors pointed out the structure-directing effect of K⁺ on MnO_x-based OER-electrocatalysts and linked this effect to significant changes in OER-performance. Our results go further in showing that in the case of Ir-oxohydroxides, an optimal amount of K is required in order to form the right structure that combines both high activity and stability under acidic OER-conditions.

Conclusions

Recent studies have highlighted the superior properties of elusive quasi-amorphous or nanocrystalline Ir-oxohydroxides for OER-electrocatalysis in acidic media.^[14,16-18,35,45] In order to address this challenge, the present report proposes a MW-assisted hydrothermal synthesis protocol as a dedicated synthesis strategy for the systematic preparation of Ir-oxohydroxide powders. We identified the initial KOH:Ir-ratio as having a major effect on the final composition and chemical nature of the produced Ir-oxohydroxides. Indeed the initial KOH:Ir-ratio is suspected of strongly influencing the Ir-precursor hydrolyzation and oligomerization process preceding the

condensation of a solid product. For KOH:Ir=5:1, an essentially Cl-free and Ir⁰-free Ir-oxohydroxide Ir^{+3.5}O_{0.9}(OH)_{1.8} could be obtained at 99% synthesis yield. This compound exhibited both remarkable OER-activity and stability when compared to a commercially available Ir-oxohydroxide (AA-IrO_x) and literature reports.^[4,38]

The compositional analysis of the MW-produced Ir-oxohydroxides constitutes an important step in the understanding of this class of materials, which has so far proven elusive to characterization and difficult to synthesize in a pure form.^[33] TPR exhibited sharp low-temperature reduction features, characteristic for quasi-amorphous Ir-oxohydroxides and suggests a mixed Ir^{III/IV}-oxidation state. The comparison of OER-performances and structural features revealed the prominent role of Ir-OH-species accommodated in the particular Ir^{III/IV}-environment of Ir-oxohydroxides. K⁺-cations present in smaller amounts in the Ir-oxohydroxides obtained for KOH:Ir≤5:1 are thought to play a major role in stabilizing a high-performance Ir-oxohydroxide phase containing high amounts of OER-relevant hydroxyl groups. On the contrary, higher K-contents obtained for KOH:Ir≥7:1 lead to the formation of a distinct nanocrystalline Ir-oxohydroxide phase characterized by significantly lower stability under OER-conditions.

More in-depth investigation will be needed to understand the chemical nature of the hydroxyl groups, their link to the electrocatalytic properties of the compounds and the exact role of K⁺-cations. However these results lead us to the conclusion that the superior OER-performance of nanocrystalline Ir-oxohydroxides is prominently linked to their ability to accommodate catalytic precursor sites involving mixed Ir^{III/IV}-species stabilized in a highly hydroxylated, K-containing environment. As such, our MW-produced compounds bridge the gap between metallic Ir and crystalline IrO₂, which both need to be electrochemically activated in order to allow for appreciable electrocatalytic activity.

Furthermore, the recent investigation by Pfeifer et al. on the electronic structure of quasi-amorphous Ir-compounds pointed out the presence of OER-relevant nucleophilic O-species in the particular environment of Ir^{III/IV}-oxohydroxides.^[16–18] The presence of such reactive O-species is a likely explanation for the high reactivity of our MW-produced Ir-oxohydroxides observed with H₂ in TPR. As a result, future investigations based on XPS and XAS will focus on links between the electronic structure of our compounds, especially the presence of nucleophilic O-species and their relevance for OER-performance.

As a result this report proposes a dedicated synthesis protocol for the production of a new class of Ir-oxohydroxides that combine both activity and stability under harsh acidic OER-conditions. This study also provides several important clues on the structural features determining the OER-performance of Ir-oxohydroxides. Thus our results constitute a major step towards the targeted design of Ir-based OER-electrocatalysts for economically viable energy storage based on PEM-electrolysers.

Experimental Section

Synthesis.— Ir-compounds were prepared via MW-assisted hydrothermal treatment of aqueous precursor solutions containing dissolved potassium hexachloroiridate(IV) (K₂IrCl₆, Alfa Aesar, Ir 39% min.) and KOH in predefined KOH:Ir-ratios. A series of seven samples were prepared from precursor solutions with initial KOH:Ir-ratios ranging from 1:1 to 100:1 for a constant initial Ir concentration of 10⁻² mol L⁻¹. Four times 62 mL of the precursor solution were heated in four PTFE-lined vessels under continuous stirring with a ramp of 10 K min⁻¹ and maintained at 250°C, approx. 55 bar for 60 minutes (Fig. S1, in supporting

information (S.I.)) using a MW-supported hydrothermal synthesis reactor system (Anton Paar, Multiwave PRO). The vessels were then cooled to room temperature (RT) and the resulting black Ir-compounds were centrifuged at 8000 rpm for 10 min, re-suspended in milli-Q water (AppliChem, 18 MΩ, TOC < 3 ppb), sonicated for 5 minutes and re-centrifuged until the conductivity of the supernatant was measured below 0.05 mS.cm⁻¹. The powders were subsequently dried at 80°C for 12h and ground in a mortar.

Catalyst characterization.— In order to detect Ir-species remaining in solution after the MW-treatment, the supernatant of the first centrifugation was analyzed at RT in a 0.1 mm thick quartz cuvette by UV-Vis-spectroscopy (Lambda 650 UV-vis spectrometer, Perkin Elmer) from 200 to 800 nm. For the produced powders, the elemental ratios of K and Cl to Ir were obtained via X-ray fluorescence analysis (XRF, sequential Pioneer S4 spectrometer, Bruker) under inert He atmosphere. Powder X-ray diffraction (XRD) patterns were collected on a STOE STADI P diffractometer equipped with a primary focusing Ge-monochromator with Cu Kα₁ radiation and a linear position sensitive detector. The XRD samples were measured between two layers of polyacetate films maintained together with X-ray amorphous grease. Scanning Electron Microscopy (SEM, Hitachi S-4800 Field Emission Scanning Electron Microscope) images were captured in the kV-range of 0.1 to 30. The SEM was equipped with low angle (LA) and YAG-BSE detectors for atomic number-sensitive secondary electron detection. The specific surface area of the catalysts was quantified by static nitrogen physisorption (Quantachrome, Autosorb-1C) using a standard multipoint method to derive the specific surface area from the measured isotherm. For high resolution transmission electron microscopy (HRTEM) and scanning transmission electron microscopy (STEM), samples were prepared by casting two drops of aqueous sample solution on carbon-coated Cu grids. (S)TEM images and energy-dispersive X-ray spectroscopic (EDX) elemental mapping were performed on an aberration-corrected JEOL JEM-ARM200 operated at 200 kV. The microscope is equipped with a high angle Silicon Drift EDX detector with the solid angle of up to 0.98 steradians from a detection area of 100 mm². The thermal decomposition of the samples was studied using thermogravimetric analysis (TGA, Netzsch STA 449 thermobalance) with simultaneous evolved gas analysis using a quadrupole mass spectrometer (QMS200 Omnistar, Balzers). Typically, the samples were heated at 10Kmin⁻¹ from RT to 800 °C in a 21%-O₂/Ar atmosphere (100mL min⁻¹). Temperature programmed reduction (TPR) of the samples was performed in a fixed-bed reactor in a 4.92 vol.% H₂/Ar-flow (80 mL min⁻¹) using a heating rate of 6 K min⁻¹ from RT to 450°C. The H₂-consumption was monitored using a thermal conductivity detector (TCD, X-stream gas analyzer, Emerson).

Electrochemical measurements.— The electrochemical measurements were performed at RT in a standard three-compartment cell containing 100 mL H₂SO₄ (0.5 mol L⁻¹) electrolyte constantly purged with N₂. The OER-performance was evaluated using a multichannel potentiostat (BioLogic EC-Lab, VSP-300) with a glassy carbon (GC) rotating disk electrode (RDE, 0.2475 cm², Pine Research Instrumentation) as a working electrode. A Pt-wire was used as a counter electrode and a saturated calomel electrode (SCE) at +0.241V vs. Standard Hydrogen Electrode (SHE) as a reference electrode. Prior to use, the GC support was mirror-polished with alumina bead slurries (Buehler, 1 μm and 0.05 μm) on a polishing cloth, rinsed with milli-Q water, cleaned for 15 min in isopropanol in an ultrasonic bath and finally rinsed with milli-Q water and isopropanol. The catalyst inks were prepared by suspending 4 mg of powder in 6 mL milli-Q water, 3.96 mL isopropanol and 40 μL of Nafion (5%-Nafion, Sigma Aldrich). Typically, 20-100 μg_{Ir} cm⁻² (geometrical area) were drop-casted onto the GC disk using a micropipette and dried for 30 min at 60°C. Significant

contributions to the observed current densities from the RDE or the blank catalyst ink can be neglected as shown by the LSV of the pristine RDE and the RDE loaded with blank ink (Fig. S11). The electrochemical results are compared to two commercially available benchmarks that are quasi-amorphous ultrapure iridium oxohydroxide (Ir^{IV} oxide, Premion, 99.99% trace metals basis, Ir 84.5% min, Alfa Aesar) labeled "AA-IrO_x" and crystalline IrO₂ (99.9% trace metals basis, Sigma Aldrich) labeled "SA-IrO₂". The extensive characterization of these samples is reported elsewhere.^[16]

All electrochemical measurements were corrected at 85% for ohmic drop using high-frequency impedance spectroscopy (4 measurements, 100 kHz, 20 mV amplitude, open circuit potential, E_{oc}). The catalyst activity was assessed using linear sweep voltammetry (LSV) performed at a sweep rate of 5 mV s⁻¹ from open circuit potential (E_{oc}) to 2 V vs. SHE. The overpotential needed to reach a current of j = 10 mA cm⁻² was used as a measure of the activity. The overpotential has been determined according to Eq. (1) where η is the overpotential and E the working electrode potential vs. SHE.

$$\eta = E - (1.23 - 0.059 \times p\text{H}) \quad (1)$$

In order to assess catalyst stability, chronopotentiometric (CP) testing was performed under severe experimental conditions at current densities of 15 mA cm⁻² for Ir-loadings of 20 μg_{Ir} cm⁻². The stability of the best electrocatalyst was further assessed at current densities of 10 mA cm⁻² for three Ir-loadings (20, 50 and 100 μg_{Ir} cm⁻²) in order to allow for comparison with benchmarks reported in the literature.^[4,38] A current density of 10 mA cm⁻² is based on the typical currents expected for a 10%-efficiency solar-to-fuel device.^[4,46] The catalyst were considered deactivated when E reached 1.8 V vs. SHE in order to avoid oxidative damage to the GC-electrode support.

Acknowledgements

Financial support came from the German Federal Ministry for Economic Affairs and Energy (BMWi) in the framework of the "Ekolyser"-project (n° 03ESP106D). We thank Jasmin Allan, Wiebke Frandsen and Maike Hashagen for their help with various characterization methods.

Keywords: iridium • oxygen evolution reaction • electrocatalysis • water splitting • chemical energy storage

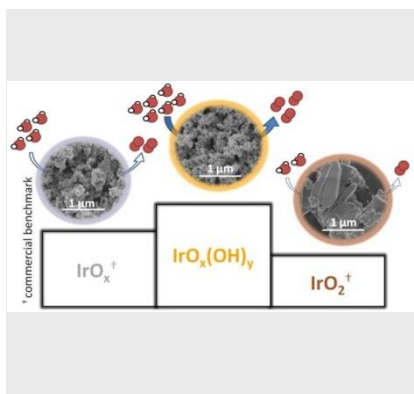
- [1] R. Schlögl, *ChemSusChem* **2010**, *3*, 209–222.
- [2] M. Carmo, D. L. Fritz, J. Mergel, D. Stolten, D. L. F. Marcelo Carmo, *Int. J. Hydrogen Energy* **2013**, *38*, 4901–4934.
- [3] I. Katsounaros, S. Cherevko, A. R. Zeradjanin, K. J. J. Mayrhofer, *Angew. Chem.* **2014**, *126*, 104–124; *Angew. Chem. Int. Ed.* **2014**, *53*, 102–121.
- [4] C. C. L. McCrory, S. Jung, I. M. Ferrer, S. M. Chatman, J. C. Peters, T. F. Jaramillo, *J. Am. Chem. Soc.* **2015**, *137*, 4347–4357.
- [5] S. R. Taylor, *Geochim. Cosmochim. Acta* **1964**, *28*, 1273–1285.
- [6] G. Beni, L. M. Schiavone, J. L. Shay, W. C. Dautremont-Smith, B. S. Schneider, *Nature* **1979**, *282*, 281–283.
- [7] E. J. Frazer, R. Woods, *J. Electroanal. Chem. Interfacial Electrochem.* **1979**, *102*, 127–130.
- [8] M. Vuković, *J. Appl. Electrochem.* **1987**, *17*, 737–745.
- [9] R. Mráz, J. Krýsa, *J. Appl. Electrochem.* **1994**, *24*, 1262–1266.
- [10] L. K. Xu, J. D. Scantlebury, *Corros. Sci.* **2003**, *45*, 2729–2740.
- [11] L. K. Xu, J. D. Scantlebury, *J. Electrochem. Soc.* **2003**, *150*, B254–B261.
- [12] L. Xu, Y. Xin, J. Wang, *Electrochim. Acta* **2009**, *54*, 1820–1825.
- [13] J. O. Bockris, T. Otagawa, *J. Electrochem. Soc.* **1984**, *131*, 290–302.
- [14] T. Reier, D. Teschner, T. Lunkenbein, A. Bergmann, S. Selve, R. Kraehnert, R. Schlögl, P. Strasser, *J. Electrochem. Soc.* **2014**, *161*, F876–F882.
- [15] T. Reier, Z. Pawolek, S. Cherevko, M. Bruns, T. Jones, D. Teschner, S. Selve, A. Bergmann, H. N. Nong, R. Schlögl, et al., *J. Am. Chem. Soc.* **2015**, *137*, 13031–13040.
- [16] V. Pfeifer, T. E. Jones, J. J. Velasco Vélez, C. Massué, R. Arrigo, D. Teschner, F. Girgsdies, M. Scherzer, M. T. Greiner, J. Allan, et al., *Surf. Interface Anal.* **2016**, *48*, 261–273.
- [17] V. Pfeifer, T. E. Jones, J. J. Velasco Vélez, C. Massué, M. T. Greiner, R. Arrigo, D. Teschner, F. Girgsdies, M. Scherzer, J. Allan, et al., *Phys. Chem. Chem. Phys.* **2016**, *18*, 2292–2296.
- [18] V. Pfeifer, T. E. Jones, S. Wrabetz, C. Massue, J. J. Velasco Velez, R. Arrigo, M. Scherzer, S. Piccinin, M. Havecker, A. Knop-Gericke, et al., *Chem. Sci.* **2016**, *7*, 6791–6795.
- [19] F. Conrad, C. Massue, S. Kühl, E. Kunkes, F. Girgsdies, I. Kasatkin, B. Zhang, M. Friedrich, Y. Luo, M. Armbrüster, et al., *Nanoscale* **2012**, *4*, 2018–2028.
- [20] T. Ioroi, N. Kitazawa, K. Yasuda, Y. Yamamoto, H. Takenaka, *J. Electrochem. Soc.* **2000**, *147*, 2018–2022.
- [21] K. R. Rodgers, H. Gamsjäger, R. K. Murmann, *Inorg. Chem.* **1989**, *28*, 379–381.
- [22] Y. Zhao, N. M. Vargas-Barbosa, M. E. Strayer, N. S. McCool, M.-E. Pandelia, T. P. Saunders, J. R. Swierk, J. F. Callejas, L. Jensen, T. E. Mallouk, *J. Am. Chem. Soc.* **2015**, *137*, 8749–8757.
- [23] L. Moggi, G. Varani, M. F. Manfrin, V. Balzani, *Inorganica Chim. Acta* **1970**, *4*, 335–341.
- [24] I. A. Poulsen, C. S. Garner, *J. Am. Chem. Soc.* **1962**, *84*, 2032–2037.
- [25] P. Beutler, H. Gamsjäger, *J. Chem. Soc., Chem. Commun.* **1976**, 554–555.
- [26] H. Gamsjäger, P. Beutler, *J. Chem. Soc. Dalt. Trans.* **1979**, *9*, 1415–1418.
- [27] S. E. Castillo-Blum, D. T. Richens, A. G. Sykes, *J. Chem. Soc. Chem. Commun.* **1986**, 1120–1121.
- [28] D. A. Pankratov, P. N. Komozin, Y. M. Kiselev, *Russ. J. Inorg. Chem.* **2011**, *56*, 1794–1799.
- [29] C. P. De Pauli, S. Trasatti, *J. Electroanal. Chem.* **2002**, 538–539, 145–151.
- [30] J. M. Hu, H. M. Meng, J. Q. Zhang, C. N. Cao, *Corros. Sci.* **2002**, *44*, 1655–1668.
- [31] J. Krýsa, J. Maixner, R. Mraz, I. Rousar, *J. Appl. Electrochem.* **1998**, *28*, 369–372.
- [32] P. Lettenmeier, L. Wang, U. Golla-Schindler, P. Gazdzicki, N. A. Cañas, M. Handl, R. Hiesgen, S. S. Hosseiny, A. S. Gago, K. A. Friedrich, *Angew. Chemie* **2016**, *128*, 752–756; *Angew. Chem. Int. Ed.* **2016**, *55*, 742–746.
- [33] A. M. Cruz, L. Abad, N. M. Carretero, J. Moral-Vico, J. Fraxedas, P. Lozano, G. Subías, V. Padial, M. Carballo, J. E. Collazos-Castro, et al., *J. Phys. Chem. C* **2012**, *116*, 5155–5168.
- [34] N. M. Carretero, M. P. Lichtenstein, E. Pérez, L. Cabana, C. Suñol, N. Casañ-Pastor, *Acta Biomater.* **2014**, *10*, 4548–4558.
- [35] D. F. Abbott, D. Lebedev, K. Waltar, M. Povia, M. Nachttegaal, E. Fabbri, C. Copéret, T. J. Schmidt, *Chem. Mater.* **2016**, *28*, 6591–6604.
- [36] N. Bestaoui, E. Prouzet, *Chem. Mater.* **1997**, *9*, 1036–1041.
- [37] S. H. Brewer, D. Wicaksana, J.-P. Maria, A. I. Kingon, S. Franzen, *Chem. Phys.* **2005**, *313*, 25–31.
- [38] C. C. L. McCrory, S. Jung, J. C. Peters, T. F. Jaramillo, *J. Am. Chem. Soc.* **2013**, *135*, 16977–16987.
- [39] S. Trasatti, *Electrochim. Acta* **1984**, *29*, 1503–1512.
- [40] T. Shinagawa, A. T. Garcia-Esparza, K. Takanabe, *Sci. Rep.* **2015**, *5*, 13801.
- [41] Y. Yi, J. Tornow, E. Willinger, M. G. Willinger, C. Ranjan, R. Schlögl, *ChemElectroChem* **2015**, *2*, 1929–1937.
- [42] S. Cherevko, T. Reier, A. R. Zeradjanin, Z. Pawolek, P. Strasser, K. J. J. Mayrhofer, *Electrochem. Commun.* **2014**, *48*, 81–85.
- [43] J. M. Spurgeon, J. M. Velazquez, M. T. McDowell, *Phys. Chem. Chem. Phys.* **2014**, *16*, 3623–3631.
- [44] Q. Gao, C. Ranjan, Z. Pavlovic, R. Blume, R. Schlögl, *ACS Catal.* **2015**, *5*, 7265–7275.
- [45] A. Minguzzi, C. Locatelli, O. Lugaresi, E. Achilli, G. Cappelletti, M. Scavini, M. Coduri, P. Masala, B. Sacchi, A. Vertova, et al., *ACS Catal.* **2015**, *5*, 5104–5115.
- [46] Y. Gorlin, T. F. Jaramillo, *J. Am. Chem. Soc.* **2010**, *132*, 13612–13614.

Entry for the Table of Contents

Layout 1:

FULL PAPER

We report the synthesis of a new class of amorphous Ir-oxohydroxide water oxidation electrocatalysts, presenting unprecedented performance in acidic media at loadings low enough for commercial application. Such novel materials achieved 33 times longer lifetimes than the best commercial benchmark available and thus constitute a major advance in the rational design of efficient OER-catalysts for acidic water electrolysis.



Cyriac Massué, Xing Huang, Andrey Tarasov, Chinmoy Ranjan, Sébastien Cap* and Robert Schlögl

Page No. – Page No.
Microwave Assisted Synthesis of Stable and Highly Active Ir-oxohydroxides for Electrochemical Oxidation of Water